J. Cent. South Univ. (2015) 22: 2971−2979
DOI: 10.1007/s11771-015-2833-y

Springer

Elastodynamic modeling and joint reaction prediction for 3-PRS PKM

ZHANG Jun(张俊)[1, 2], ZHAO Yan-qin(赵艳芹)[1]

1.School of Mechanical Engineering, Anhui University of Technology, Ma'anshan 243032, China;
2. State Key Laboratory of High Performance Complex Manufacturing
(Central South University), Changsha 410083, China

Abstract: To gain a thorough understanding of the load state of parallel kinematic machines (PKMs), a methodology of elastodynamic modeling and joint reaction prediction is proposed. For this purpose, a Sprint Z3 model is used as a case study to illustrate the process of joint reaction analysis. The substructure synthesis method is applied to deriving an analytical elastodynamic model for the 3-PRS PKM device, in which the compliances of limbs and joints are considered. Each limb assembly is modeled as a spatial beam with non-uniform cross-section supported by lumped virtual springs at the centers of revolute and spherical joints. By introducing the deformation compatibility conditions between the limbs and the platform, the governing equations of motion of the system are obtained. After degenerating the governing equations into quasi-static equations, the effects of the gravity on system deflections and joint reactions are investigated with the purpose of providing useful information for the kinematic calibration and component strength calculations as well as structural optimizations of the 3-PRS PKM module. The simulation results indicate that the elastic deformation of the moving platform in the direction of gravity caused by gravity is quite large and cannot be ignored. Meanwhile, the distributions of joint reactions are axisymmetric and position-dependent. It is worthy to note that the proposed elastodynamic modeling method combines the benefits of accuracy of finite element method and concision of analytical method so that it can be used to predict the stiffness characteristics and joint reactions of a PKM throughout its entire workspace in a quick and accurate manner. Moreover, the present model can also be easily applied to evaluating the overall rigidity performance as well as statics of other PKMs with high efficiency after minor modifications.

Key words: parallel kinematic machine (PKM); 3-PRS PKM; Sprint Z3 head; elastodynamic modeling; joint reaction

1 Introduction

Parallel kinematic machines (PKMs) have been proposed as an alternative solution for high-speed machining tool for years due to the merits of simple structure, high rigidity, better accuracy, good reconfigurability and easy controlling. This has been fully exemplified by the commercial success of Sprint Z3 head applied in aeronautical industries [1] and the Tricept robots used in locomotive industries [2−3].

As a multiple-axis spindle head with 1T2R capacity, Sprint Z3 head has aroused great interests from industrial and academic fields since its invention. The topological architecture of Sprint Z3 head is a 3-PRS parallel mechanism. Extensive investigations have been carried out on the 3-PRS parallel mechanism, ranging from inverse and forward kinematics [4−5], workspace prediction [6−7], Jacobian formulation [8], parasitic motion [9] to stiffness evaluation [10−11] and rigid-body dynamics [12−13]. Despite numerous researches mentioned above, investigations on dynamics and load state of the 3-PRS parallel mechanism are quite scare as far as the author's knowledge is concerned. Nevertheless, the dynamic performance evaluation and kinematic pair load prediction are two main concerns in the design stage of such a PKM module used for high-speed machining where high accuracy is required.

As evidenced by the literature, the dynamic modelling of PKMs has been gradually addressed. In the first stage, equations of motion for the PKMs were derived with assumptions that all components are rigid bodies [14−16]. The Kane's method was commonly used in these models due to the closed-loop kinematic chains property of PKMs. In the early 1990s, LEE and GENG [17] derived the Lagrange equations for flexible 6-RPR spatial manipulators using tensor representation, in which the piston was modelled as a mass-spring-damper. Much literature along this track can be found in Refs. [18−20]. However, it is worthy to point out that in

Foundation item: Project(Kfkt2013-12) supported by Open Research Fund of Key Laboratory of High Performance Complex Manufacturing of Central South University, China; Project(2014002) supported by the Open Fund of Shanghai Key Laboratory of Digital Manufacture for Thin-walled Structures, China; Project(51375013) supported by the National Natural Science Foundation of China
Received date: 2014−07−30; **Accepted date:** 2014−11−15
Corresponding author: ZHANG Jun, PhD, Professor; Tel: +86−18855521039; E-mail: zhang_jun@tju.edu.cn

the aforementioned literature joint stiffnesses were not taken into account yet they would bring significant influences on the global stiffness and dynamics of the system. SHIAU et al [21] proposed a nonlinear dynamic model for a 3-PRS PKM, in which the limbs were treated as rigid and the joints were simplified as isotropic constant springs.

From the above discussions, it can be seen that the component stiffnesses are crucial to system dynamics and should be modelled dedicatedly when establishing a dynamic model for such PKMs. Considering the 3-PRS module as a compliant parallel mechanism where the three PRS limbs are equivalent to three sets of springs that have bending, extending and torsional deflections, a comprehensive elastodynamic model for the 3-PRS PKM module is presented. Based on the proposed elastodynamic model, the quasi-static equations are derived by degenerating the differential term in the governing equations of motion. The analysis is then extended to the prediction of joint reactions in order to provide the designer with useful information in the stage of structural design.

2 Kinematic description of 3-PRS PKM

A CAD model for a Sprint Z3 head is shown in Fig. 1, which consists of a moving platform, a fixed base and three identical PRS limb assemblies. Each PRS limb assembly consists of a hollowed limb body with non-uninform cross-sections, a carriage containing ball screw assembly driven by a servo motor, and a fixed base with a guideway. An electrical spindle is mounted on the platform to implement high-speed milling. Independently driven by three servomotors, one translation along z axis and two rotations about x and y axes can be achieved.

As can be seen from Fig. 1, the topological architecture of Sprint Z3 head is a 3-PRS parallel

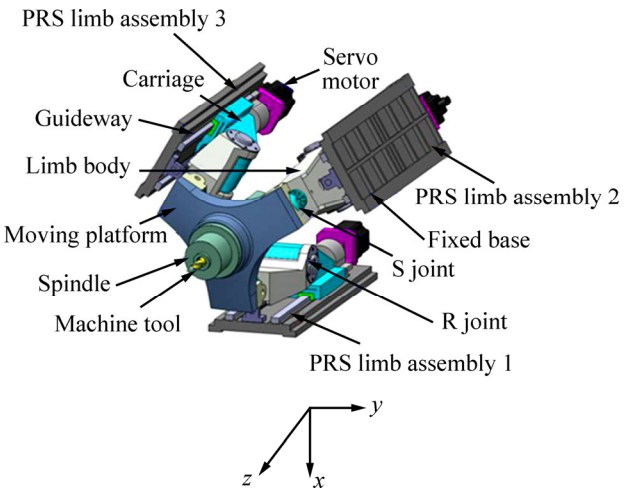

Fig. 1 Structure of 3-PRS PKM module

mechanism. To facilitate the formulations, the schematic diagram and corresponding coordinates of the 3-PRS PKM are depicted in Fig. 2.

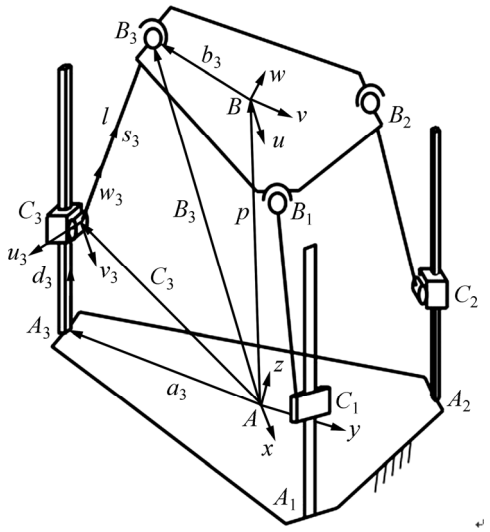

Fig. 2 Schematic diagram of 3-PRS PKM module

Herein, B_i and C_i (i=1, 2, 3) are the centers of spherical and revolute joints, respectively; A_i denotes the rear end of the limb (also is the installation point of rear bearing); $\Delta A_1A_2A_3$ and $\Delta B_1B_2B_3$ are assumed to be equilateral. To facilitate the formulation, Cartesian coordinate systems are set as the followings. A global Cartesian coordinate system A-xyz is attached on the centre point A of the fixed base, in which x axis is set along the direction of AA_1 and z axis is perpendicular to the plane $A_1A_2A_3$ while y axis is decided with the right-hand rule. Similarly, a body-fixed moving Cartesian coordinate system B-uvw is set at the centre point B of the moving platform, in which u is in the direction of BB_1 and w is perpendicular to the plane $B_1B_2B_3$ while v is decided according to the right-hand rule. Meanwhile, a limb reference coordinate frame C_i-$u_iv_iw_i$ (i=1,2,3) is established at the centre point C_i of the i-th revolute joint, in which u_i and w_i are coincident with the axes of revolute joint and limb body, respectively, while v_i is determined with the right-hand rule. For clarity, only one limb reference frame in limb 3 is depicted in Fig. 2.

The transformation matrix $\boldsymbol{R}_0$ of the frame B-uvw with respect to the frame A-xyz can be formulated as

$$\boldsymbol{R}_0 = [\boldsymbol{R}_{01} \quad \boldsymbol{R}_{02} \quad \boldsymbol{R}_{03}] = \begin{bmatrix} \cos\psi\cos\phi-\sin\psi\cos\theta\sin\phi & -\cos\psi\sin\phi-\sin\psi\cos\theta\cos\phi & \sin\psi\sin\theta \\ \sin\psi\cos\phi+\cos\psi\cos\theta\sin\phi & -\sin\psi\sin\phi+\cos\psi\cos\theta\cos\phi & -\cos\psi\sin\theta \\ \sin\theta\sin\phi & \sin\theta\cos\phi & \cos\theta \end{bmatrix} \tag{1}$$

where ψ, θ and ϕ are Euler angles in terms of precession, nutation and rotation, respectively.

The position vector of point B_i measured in the

global coordinate system *A-xyz* can be given as

$$\boldsymbol{B}_i = \boldsymbol{R}_0\boldsymbol{b}_i + \boldsymbol{p} = \boldsymbol{a}_i + d_i\boldsymbol{n} + l\boldsymbol{s}_i \tag{2}$$

where $\boldsymbol{b}_i$ and $\boldsymbol{p}$ are the vectors of point B_i and point B measured in *B-uvw* and *A-xyz* respectively; $\boldsymbol{a}_i$ is the vector of point A_i measured in *A-xyz* and d_i is the stroke of the *i*-th slider measuring from point A_i to C_i; l is the length of limb body; $\boldsymbol{n}$ is the unit vector of guideway and $\boldsymbol{s}_i$ is the unit vector of $\boldsymbol{C}_i\boldsymbol{B}_i$ measured in the frame of *A-xyz*. There exist

$$\boldsymbol{b}_i = r_{\mathrm{p}}\begin{pmatrix}\cos\beta_i\\ \sin\beta_i\\ 0\end{pmatrix}, \boldsymbol{a}_i = r_{\mathrm{b}}\begin{pmatrix}\cos\beta_i\\ \sin\beta_i\\ 0\end{pmatrix}, \boldsymbol{p} = \begin{pmatrix}p_x\\ p_y\\ p_z\end{pmatrix}, \boldsymbol{n} = \begin{pmatrix}0\\ 0\\ 1\end{pmatrix} \tag{3}$$

where r_{p} and r_{b} are the radii of the moving platform and the fixed base, respectively; $\beta_i = 2\pi(i-1)/3$ are the position angles of the revolute joints; p_x, p_y and p_z are coordinates of point B measured in frame *A-xyz*.

Taking ψ, θ and p_z as independent coordinates, and considering the constrains of revolute joints, one can obtain

$$\begin{cases} p_x = 0.5r_{\mathrm{p}}(1-\cos\theta)\cos(2\psi) \\ p_y = -0.5r_{\mathrm{p}}(1-\cos\theta)\sin(2\psi) \\ \phi = -\psi \end{cases} \tag{4}$$

Noting that

$$\left|\boldsymbol{C}_i\boldsymbol{B}_i\right| = l \tag{5}$$

Solving Eq. (5), one can derive the inverse kinematics of the PKM model.

3 Elastodynamic modeling

Considering the structural features of the 3-PRS PKM module, one can decompose the PKM system into one fixed base subsystem, one moving platform subsystem and three identical limb subsystems. For the convenience of analytical derivation, the following hypotheses and approximations are made.

1) The base and the moving platform are treated as rigid bodies due to their relatively high rigidities;

2) The limb body is modeled as a continuum elastic hollowed spatial beam with non-uniform cross-sections according to its structural feature;

3) The revolute and spherical joints are simplified into virtual lumped springs with equivalent stiffness at their geometric centres;

4) The transient structural assumption is adopted and the coupling effect between rigid and elastic motions is negligible as the mechanism works at low or moderate speed;

5) Clearances, frictions and dampings in joints are neglected though they can be added to the governing equations in an easy way.

3.1 Dynamic modelling of PRS limb assembly

Figure 3 shows the assemblage of a PRS limb in the 3-PRS PKM module.

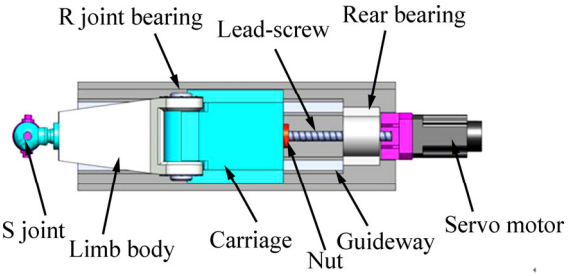

Fig. 3 Assembly of PRS limb

According to the assembling relationships and structural features of the PRS limb, one can classify all the components in an individual PRS limb into three categories when formulating the compliance expression: the limb body, the revolute joint (including the lead-screw-nut assembly and carriage-guideway assembly) and the spherical joint.

Consequently, the compliance of an entire PRS limb assembly can be regarded as a serial combination of the aforementioned three compliant components. With the knowledge of kineto-elastodynamics, one can model the hollowed PRS limb body as a non-uniform spatial beam constrained by two sets of lumped springs with equivalent stiffness as shown in Fig. 4.

The symbols in Fig. 4 are defined as follows. $k_{\mathrm{sx}i}$, $k_{\mathrm{sy}i}$ and $k_{\mathrm{sz}i}$ are the stiffness coefficients of three virtual lumped translational linear springs of the spherical joint; $k_{\mathrm{rx}i}$, $k_{\mathrm{ry}i}$, $k_{\mathrm{rz}i}$ and $k_{\mathrm{ru}i}$, $k_{\mathrm{rv}i}$, $k_{\mathrm{rw}i}$ are stiffness coefficients of the translational and torsional lumped springs of the revolute joint in the *i*-th limb assembly, respectively.

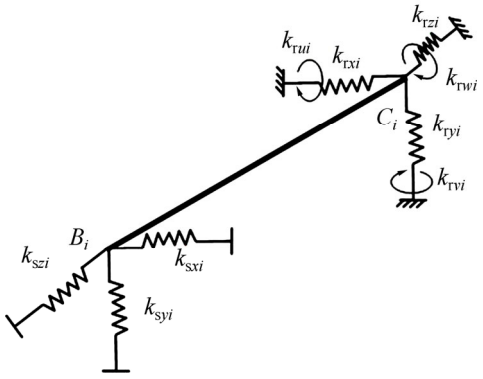

Fig. 4 Force diagram of limb body

The geometric feature of the limb body is demonstrated in Fig. 5. As shown in Fig. 5, the cross-sections of the limb body are not uniform. To be specific, the cross-section of segment B_iD_i of the limb body is in a rectangular form with gradually changing

dimensions. The topological form of the cross-section is depicted as I. Accordingly, the cross-sections of segment D_iE_i and E_iC_i are labeled as II and III, respectively. For clarity, the dimensional parameters of the cross-sections are not shown in the above figure.

As aforementioned, the limb body of the PRS limb in the PKM module can be modeled as a hollowed spatial beam with non-uniform cross-sections constrained by two sets of lumped springs. The following will derive the differential equations of motion for the limb body by finite element method.

As shown in Fig. 5, the hollowed limb body is discretized into several segments with a spatial beam element. The spatial beam element is defined by two nodes, each having three linear and three angular coordinates (along and about three axes). Figure 6 shows the e-th element of the i-th limb in element reference frame $N_i^e - x_i^e y_i^e z_i^e$. Here, e and e+1 denote two adjacent nodes of the element, u_i (i=1−12) represents the nodal coordinates and the frame of $N_i^e - x_i^e y_i^e z_i^e$ is parallel to the limb frame of C_i-$u_iv_iw_i$.

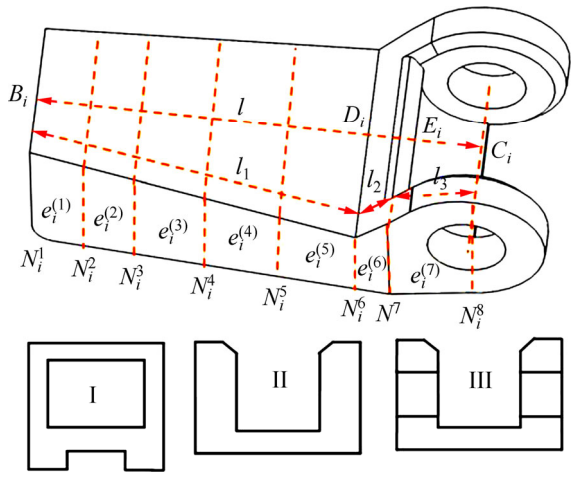

Fig. 5 Sketch of limb body cross-section

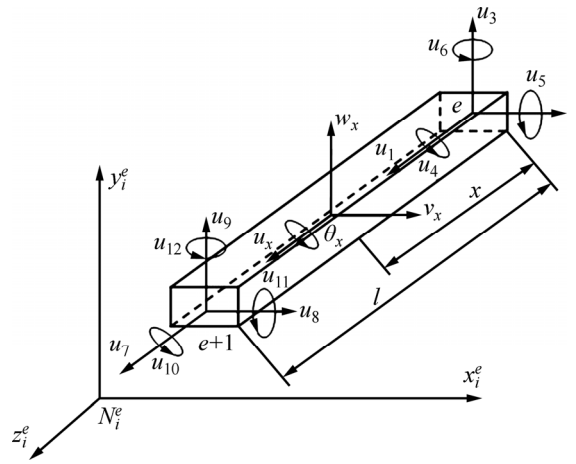

Fig. 6 Definition of spatial beam element

Consequently, a set of equations of motion of the i-th limb in the limb frame C_i-$u_iv_iw_i$ can be formulated with adequate boundary conditions. For convenience, the subscript except the limb body number i (i=1, 2, 3) is omitted.

$$\boldsymbol{m}_i\ddot{\boldsymbol{u}}_i + \boldsymbol{k}_i\boldsymbol{u}_i = \boldsymbol{f}_i \tag{6}$$

where $\boldsymbol{m}_i$ and $\boldsymbol{k}_i$ are mass and stiffness matrices of each limb body, and $\boldsymbol{u}_i$ and $\boldsymbol{f}_i$ are the general coordinates vector and external load vector of the i-th limb body and can be expressed as

$$\boldsymbol{u}_i = (\boldsymbol{\varepsilon}_{B_i}^{\mathrm{T}} \quad \boldsymbol{\xi}_{B_i}^{\mathrm{T}} \quad \cdots \quad \boldsymbol{\varepsilon}_{C_i}^{\mathrm{T}} \quad \boldsymbol{\xi}_{C_i}^{\mathrm{T}})^{\mathrm{T}} \tag{7}$$

$$\boldsymbol{f}_i = (\boldsymbol{f}_{B_i}^{\mathrm{T}} \quad \boldsymbol{0} \quad \cdots \quad \boldsymbol{f}_{C_i}^{\mathrm{T}} \quad \boldsymbol{\tau}_{C_i}^{\mathrm{T}})^{\mathrm{T}} \tag{8}$$

where $\boldsymbol{\varepsilon}_{B_i}, \boldsymbol{\xi}_{B_i}, \boldsymbol{\varepsilon}_{C_i}$ and $\boldsymbol{\xi}_{C_i}$ are linear and angular coordinates of nodes B_i and C_i in the frame of C_i-$u_iv_iw_i$, respectively; $\boldsymbol{f}_{B_i}$, $\boldsymbol{f}_{C_i}$ and $\boldsymbol{\tau}_{C_i}$ are reaction forces and moments at B_i and C_i measured in C_i-$u_iv_iw_i$, respectively. The nodal coordinates can be related to $\boldsymbol{u}_i$ by

$$\begin{cases} \boldsymbol{\varepsilon}_{B_i} = \boldsymbol{N}_{ci}^{B1}\boldsymbol{u}_i, \ \boldsymbol{\xi}_{B_i} = \boldsymbol{N}_{ci}^{B2}\boldsymbol{u}_i \\ \boldsymbol{\varepsilon}_{C_i} = \boldsymbol{N}_{ci}^{C1}\boldsymbol{u}_i, \ \boldsymbol{\xi}_{C_i} = \boldsymbol{N}_{ci}^{C2}\boldsymbol{u}_i \end{cases} \tag{9}$$

where $\boldsymbol{N}_{ci}^{B1}$, $\boldsymbol{N}_{ci}^{B2}$, $\boldsymbol{N}_{ci}^{C1}$, $\boldsymbol{N}_{ci}^{C2}$ are transformation matrices of nodes B_i and C_i with respect to $\boldsymbol{u}_i$ in the frame of C_i-$u_iv_iw_i$, respectively.

Thus, the coordinate transformation can be made to express Eq. (6) in the reference coordinate system as

$$\boldsymbol{M}_i\ddot{\boldsymbol{U}}_i + \boldsymbol{K}_i\boldsymbol{U}_i = \boldsymbol{F}_i \tag{10}$$

where $\boldsymbol{M}_i = \boldsymbol{T}_i\boldsymbol{m}_i\boldsymbol{T}_i^{\mathrm{T}}$, $\boldsymbol{K}_i = \boldsymbol{T}_i\boldsymbol{k}_i\boldsymbol{T}_i^{\mathrm{T}}$, $\boldsymbol{U}_i = \boldsymbol{T}_i\boldsymbol{u}_i$ $\boldsymbol{F}_i = \boldsymbol{T}_i\boldsymbol{f}_i$. Herein, $\boldsymbol{T}_i$ is the transformation matrix of the i-th limb body fixed frame with respect to the global reference and there exists

$$\boldsymbol{T}_i = \mathrm{diag}(\boldsymbol{R}_i, \cdots, \boldsymbol{R}_i) \tag{11}$$

where $\boldsymbol{R}_i$ is the transformation matrix of C_i-$u_iv_iw_i$ with respect to A-xyz and can be determined through the inverse kinematics.

3.2 Dynamic modeling for moving platform

The free body diagram of the moving platform is shown in Fig. 7.

From Fig. 7, the equations of motion of the moving platform can be formulated as

$$\boldsymbol{m}_{\mathrm{P}}\ddot{\boldsymbol{\varepsilon}}_{\mathrm{P}} = -\sum_{i=1}^{3}\boldsymbol{F}_{B_i} + \boldsymbol{F}_{\mathrm{P}}, \boldsymbol{I}_{\mathrm{P}}\ddot{\boldsymbol{\xi}}_{\mathrm{P}} = -\sum_{i=1}^{3}\boldsymbol{r}_i \times \boldsymbol{F}_{B_i} + \boldsymbol{\tau}_{\mathrm{P}} \tag{12}$$

where $\boldsymbol{m}_{\mathrm{P}}$ and $\boldsymbol{I}_{\mathrm{P}}$ are the mass and inertial matrices of the moving platform measured in A-xyz; $\boldsymbol{\varepsilon}_{\mathrm{P}}$ and $\boldsymbol{\xi}_{\mathrm{P}}$ are the linear and angular general coordinates of the moving platform; $\boldsymbol{F}_{B_i}$ is the reaction force vector at the interface between the moving platform and the i-th limb body; $\boldsymbol{r}_i$ is the vector pointing from point A to B_i; $\boldsymbol{F}_{\mathrm{P}}$ and

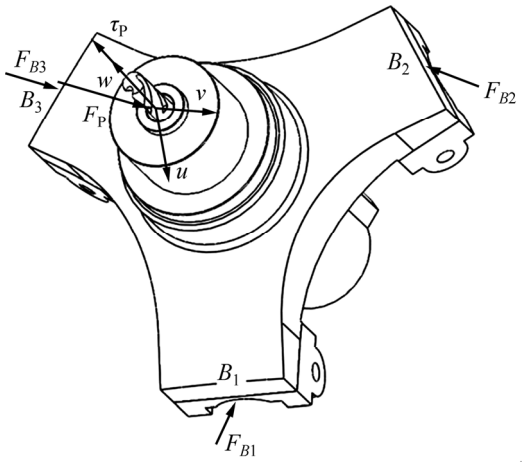

Fig. 7 Force diagram of moving platform

$\boldsymbol{\tau}_P$ are external forces and moments acting on the moving platform, respectively. And there have

$$\boldsymbol{I}_P = \boldsymbol{R}_0 \boldsymbol{I}_{P0} \boldsymbol{R}_0^T, \boldsymbol{F}_{B_i} = \boldsymbol{R}_i \boldsymbol{f}_{B_i} \tag{13}$$

where $\boldsymbol{I}_{P0}$ is the inertia of the moving platform measured in the body-fixed coordinate system B-uvw.

3.3 Deformation compatibility conditions

As mentioned above, the moving platform connects with three identical PRS limbs through three spherical joints, each of which can be treated as a virtual lumped spring with equivalent stiffness. The displacement relationship between the platform and the limb can be demonstrated as Fig. 8, in which $B_{i\mathrm{M}}$ and $B_{i\mathrm{L}}$ are the interface points associated with the moving platform and PRS limb, respectively; $\nabla \boldsymbol{B}_i$ and $\boldsymbol{\varepsilon}_{B_i}$ are displacements of $B_{i\mathrm{M}}$ and $B_{i\mathrm{L}}$ measured in the limb coordinate system C_i-$u_i v_i w_i$; $\boldsymbol{k}_{si}$ is the equivalent stiffness coefficient of the i-th spherical joint.

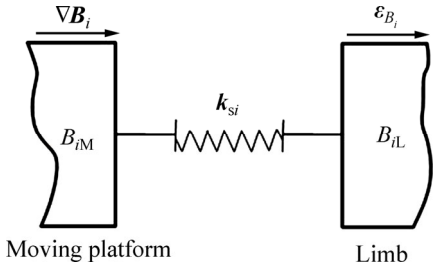

Fig. 8 Displacement relationship between platform and limb body

Observing that the elastic motion of moving platform $\boldsymbol{U}_P = (\boldsymbol{\varepsilon}_P^T, \boldsymbol{\xi}_P^T)^T$ is caused by the deflection of three flexible limbs and the platform is rigid, one can derive the elastic displacement $\nabla \boldsymbol{B}_i$ of $B_{i\mathrm{M}}$ (fixed on moving platform) as

$$\nabla \boldsymbol{B}_i = \boldsymbol{R}_i^T \boldsymbol{D}^{r_i} \boldsymbol{U}_P \tag{14}$$

where $\boldsymbol{D}^{r_i} = [\mathbf{I}_{3\times 3} \quad \hat{\boldsymbol{B}}_i]$, $\hat{\boldsymbol{B}}_i$ is the reciprocal matrix of vector $\boldsymbol{B}_i$.

Noting that the spherical joint connects the moving platform with the link at B_i, one can express the reaction forces of the spherical joint as

$$\boldsymbol{f}_{B_i} = -\boldsymbol{k}_{si}(\boldsymbol{N}_{ci}^{B1} \boldsymbol{T}_i^T \boldsymbol{U}_i - \boldsymbol{R}_i^T \boldsymbol{D}^{r_i} \boldsymbol{U}_P) \tag{15}$$

Similarly, the reactions at C_i is

$$\boldsymbol{f}_{C_i} = -\boldsymbol{k}_{r1} \boldsymbol{N}_{ci}^{C1} \boldsymbol{T}_i^T \boldsymbol{U}_i, \boldsymbol{\tau}_{C_i} = -\boldsymbol{k}_{r2} \boldsymbol{N}_{ci}^{C2} \boldsymbol{T}_i^T \boldsymbol{U}_i \tag{16}$$

where $\boldsymbol{k}_{r1} = \mathrm{diag}(k_{rx}, k_{ry}, k_{rz})$ and $\boldsymbol{k}_{r2} = \mathrm{diag}(k_{ru}, k_{rv}, k_{rw})$ are the equivalent stiffnesses of revolute joint in related directions (along and about three axes in limb reference frame $C_i - u_i v_i w_i$).

3.4 Governing equations of motion

Substituting Eqs. (15)−(16) to Eqs. (10)−(12), the governing equations of motion for the PKM system can be written as

$$\tilde{\boldsymbol{M}} \ddot{\boldsymbol{U}} + \tilde{\boldsymbol{K}} \boldsymbol{U} = \tilde{\boldsymbol{F}} \tag{17}$$

where $\tilde{\boldsymbol{K}}$ is the global stiffness matrix; $\boldsymbol{U}$ and $\tilde{\boldsymbol{F}}$ are the general coordinates and external load vectors. And there exist

$$\boldsymbol{U} = \begin{bmatrix} \boldsymbol{U}_1^T & \boldsymbol{U}_2^T & \boldsymbol{U}_3^T & \boldsymbol{U}_4^T \end{bmatrix}^T, \tilde{\boldsymbol{F}} = \begin{bmatrix} \boldsymbol{F}_1^T & \boldsymbol{F}_2^T & \boldsymbol{F}_3^T & \boldsymbol{F}_4^T \end{bmatrix}^T \tag{18}$$

$$\boldsymbol{U}_4 = (\boldsymbol{\varepsilon}_P^T \ \boldsymbol{\xi}_P^T)^T, \boldsymbol{F}_4 = (\boldsymbol{F}_P^T \ \boldsymbol{\tau}_P^T)^T \tag{19}$$

$$\tilde{\boldsymbol{K}} = \begin{pmatrix} \boldsymbol{K}_{1,1} & & & \boldsymbol{K}_{1,4} \\ & \boldsymbol{K}_{2,2} & & \boldsymbol{K}_{2,4} \\ & & \boldsymbol{K}_{3,3} & \boldsymbol{K}_{3,4} \\ \boldsymbol{K}_{4,1} & \boldsymbol{K}_{4,2} & \boldsymbol{K}_{4,3} & \boldsymbol{K}_{4,4} \end{pmatrix} \tag{20}$$

$$\boldsymbol{K}_{i,i} = \begin{pmatrix} \boldsymbol{R}_i \boldsymbol{k}_{si} \boldsymbol{N}_{ci}^{B1} \boldsymbol{T}_i^T \\ \boldsymbol{0} \\ \vdots \\ \boldsymbol{R}_i \boldsymbol{k}_{r1} \boldsymbol{N}_{ci}^{C1} \boldsymbol{T}_i^T \\ \boldsymbol{R}_i \boldsymbol{k}_{r2} \boldsymbol{N}_{ci}^{C2} \boldsymbol{T}_i^T \end{pmatrix} + \boldsymbol{K}_i \tag{21}$$

$$\tilde{\boldsymbol{M}} = \begin{bmatrix} \boldsymbol{M}_1 & & & \\ & \boldsymbol{M}_2 & & \\ & & \boldsymbol{M}_3 & \\ & & & \boldsymbol{M}_4 \end{bmatrix} \tag{22}$$

$$\boldsymbol{K}_{4,4} = \begin{pmatrix} \sum_{i=1}^{3} \boldsymbol{R}_i \boldsymbol{k}_{si} \boldsymbol{R}_i^T \boldsymbol{D}^{r_i} \\ \sum_{i=1}^{3} \boldsymbol{r}_i \times \boldsymbol{R}_i \boldsymbol{k}_{si} \boldsymbol{R}_i^T \boldsymbol{D}^{r_i} \end{pmatrix} \tag{23}$$

$$\boldsymbol{M}_4 = \begin{bmatrix} \boldsymbol{m}_P & \\ & \boldsymbol{I}_P \end{bmatrix} \tag{24}$$

$$\boldsymbol{K}_{i,4}=\begin{pmatrix}-\boldsymbol{R}_i\boldsymbol{k}_{si}\boldsymbol{R}_i^{\mathrm{T}}\boldsymbol{D}^{r_i}\\ \boldsymbol{0}\end{pmatrix} \tag{25}$$

$$\boldsymbol{K}_{4,i}=\begin{pmatrix}-\boldsymbol{R}_i\boldsymbol{k}_{si}\boldsymbol{N}_{ci}^{B1}\boldsymbol{T}_i^{\mathrm{T}}\\ -\boldsymbol{r}_i\times\boldsymbol{R}_i\boldsymbol{k}_{si}\boldsymbol{N}_{ci}^{B1}\boldsymbol{T}_i^{\mathrm{T}}\end{pmatrix} \tag{26}$$

4 Joint reactions prediction

In this section, the reaction forces of spherical and revolute joints in the 3-PRS PKM module at a given external load such as the gravity are investigated through a quasi-static analysis. The main parameters of the PKM are listed in Table 1. Herein, s denotes the stroke of the moving platform. k_{su}, k_{sv}, k_{sw}, k_{lu}, k_{lv}, k_{lw}, k_{cu}, k_{cv} and k_{cw} are stiffness coefficients of three perpendicular axes of the spherical joint in its local frame; others have been defined before. According to the parameters of the example system, the following numerical simulation and analysis can be conducted.

Table 1 Parameters of PKM

Parameter	Value
r_p/mm	250
r_b/mm	350
l/mm	550
s/mm	200
k_{su}/(N·μm^{-1})	23
k_{sv}/(N·μm^{-1})	23
k_{sw}/(N·μm^{-1})	623
k_{lu}/(N·μm^{-1})	112
k_{lv}/(N·μm^{-1})	214
k_{lw}/(N·μm^{-1})	100
k_{cu}/(N·μm^{-1})	676
k_{cv}/(N·μm^{-1})	446
k_{cw}/(N·μm^{-1})	348
k_{rx}/(N·μm^{-1})	280
k_{ry}/(N·μm^{-1})	330
k_{rz}/(N·μm^{-1})	330
k_{rv}/(MN·m·rad^{-1})	20
k_{rw}/(MN·m·rad^{-1})	20

4.1 Quasi-static deformation formulation

Note that the PKM module works at low or moderate speeds, the differential item in Eq. (17) is comparatively small thus can be omitted without causing non-negligible errors when calculating the kinematic pair reactions. Therefore, the elastodynamic equation in Eq. (17) can be simplified as

$$\tilde{\boldsymbol{K}}\boldsymbol{U}=\tilde{\boldsymbol{F}} \tag{27}$$

Equation (27) can be rewritten as

$$\boldsymbol{U}=\tilde{\boldsymbol{K}}^{-1}\tilde{\boldsymbol{F}} \tag{28}$$

Once the external load of the PKM module $\tilde{\boldsymbol{F}}$ is given and the global stiffness matrix $\tilde{\boldsymbol{K}}$ is determined by Eq. (20), the global coordinates, i.e., the elastic deformations of each component can be decided. Inserting $\boldsymbol{U}$ into Eqs. (15) and (16), one can easily obtain the reaction forces of spherical and revolute joints of the PKM module.

4.2 Gravity-caused elastic deformations

Equation (28) gives the analytical formulation for elastic deformations in the 3-PRS PKM module. This subsection will discuss the elastic displacements of the moving platform aroused from component deformations due to the gravity.

Generally speaking, the cutting force is quite small during high speed machining. Compared with the cutting force, the gravity of the moving platform and limb structures; however, it is comparably large and may bring considerable effect on the elastic displacement of the moving platform, which in turn will degenerate the machining quality of the workpiece.

According to the 3D CAD model shown in Fig. 1, the gravity of the moving platform and limb structures at the top position is calculated as 178.65 kg. By solving Eq. (28), the displacements of the moving platform can be determined and listed in the following Table.

Table 2 Elastic displacement of moving platform caused by gravity (p_z=875 mm, θ=0°, ψ=0°)

Parameter	Value
ε_{px}/μm	363.67
ε_{py}/μm	0
ε_{pz}/μm	−3.1786
ξ_{px}/10^{-4}rad	0
ξ_{py}/10^{-4}rad	−3.0686
ξ_{pz}/10^{-4}rad	0

From the above table, it can be observed that the gravity of the PKM arouses a translational displacement in the vertical direction (along x axis). The value of this deflection reaches 363.67 μm, which is not negligible during high speed machining. This translational deflection brings a rotational deflection about v axis, which is coincident with the parasitic motions of the 3-PRS mechanism as expressed in Eq. (4). Meanwhile, the gravity also causes a translational deflection along axial direction (along z axis).

4.3 Gravity-caused joint reactions

With the elastic displacements obtaining from Eq. (28), the joint reaction forces can be easily

determined by inserting $\boldsymbol{U}$ into Eqs. (15) and (16). The following tables list the reaction forces of the spherical and revolute joints caused by the gravity at the aforementioned configuration of top position.

From Table 3, it can be found that the joint reaction forces caused by the gravity are not equally distributed in three identical limbs. Taking the spherical joint for example, the S joints in three limbs all claim the biggest amplitudes in the direction of z axis (i.e. axial direction of the limb body). Among them, the S joint in limb assembly 1 has the highest value. Compared with the forces in z direction, the reactions of S joint in the other directions are smaller. Interestingly, forces distributed in the S joint in limb assembly 2 and limb assembly 3 are equal to each other in the same directions.

Table 3 Reaction forces in S joints caused by gravity (p_z=875 mm, θ=0°, ψ=0°)

Limb No	f_{Bix}/N	f_{Biy}/N	f_{Biz}/N
1	0	−0.0010	4240.5
2	−1007.6	0	−2274.5
3	1007.6	0	−2274.5

Table 4 Reaction forces in R joints caused by gravity (p_z=875 mm, θ=0°, ψ=0°)

Limb No.	f_{Cix}/N	f_{Ciy}/N	f_{Ciz}/N	τ_{Ciy}/(N·m)	τ_{Ciz}/(N·m)
1	0	0.0010	−4240.5	0	0
2	1007.6	0	2274.5	−423.2027	0
3	−1007.6	0	2274.5	423.2027	0

The reactions of revolute joints in the PKM can be found in Table 4. As to the revolute joint in limb assembly 1, the gravity only causes reactions in two directions, i.e. forces along y axis and z axis. However, the reactions are much more complicated in the revolute joints in limb assemblies 2 and 3. The gravity causes reaction forces in two directions and reaction moments about one direction. Moreover, the reactions in the same direction share the same amplitude for the revolute joints in limbs 2 and 3. This can be explained by the axial symmetry of the 3-PRS parallel configuration. Comparing Tables 3 and 4, it can be found that reactions of the spherical joint and revolute joint in the same limb claim the same value in corresponding axes.

The following will discuss the effects of configurational parameters on joint reactions due to the gravity. For content limitation, only the load distributions of spherical and revolute joints in limb assembly 1 are illustrated.

Figure 9 gives the distributions of reaction forces along three axes in the spherical joint of limb assembly 1.

Apparently, the distributions of reaction forces in three directions are strongly dependent on the

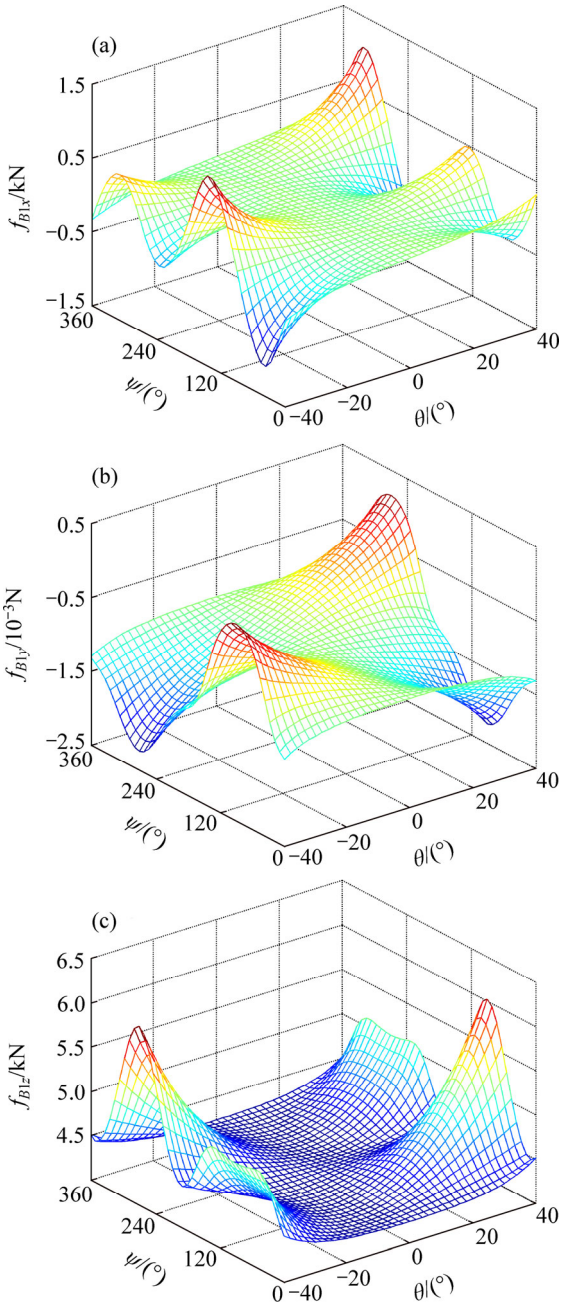

Fig. 9 Distributions of reactions in S joint over working plane at p_z=875 mm: (a) Reaction along x axis; (b) Reaction along y axis; (c) Reaction along z axis

configurational parameters. The amplitudes of each reaction force vary with the nutation angle θ and the precession angle ψ. For instance, the reaction force along x axis f_{B1x} varies from the minimal value of -1.08×10^3 to the maximal value of 1.08×10^3. The reaction force along z axis f_{B1z} changes from 4.20×10^3 to 6.02×10^3. Once again, an axisymmetric distribution over the given work plane can be observed, i.e. 40° symmetrical about the x axis, which is coincident with the axial symmetry of the structure of three RPS limbs in the 3-PRS parallel mechanism. The same tendency of load distributions can be found in revolute joints as shown in Fig. 10.

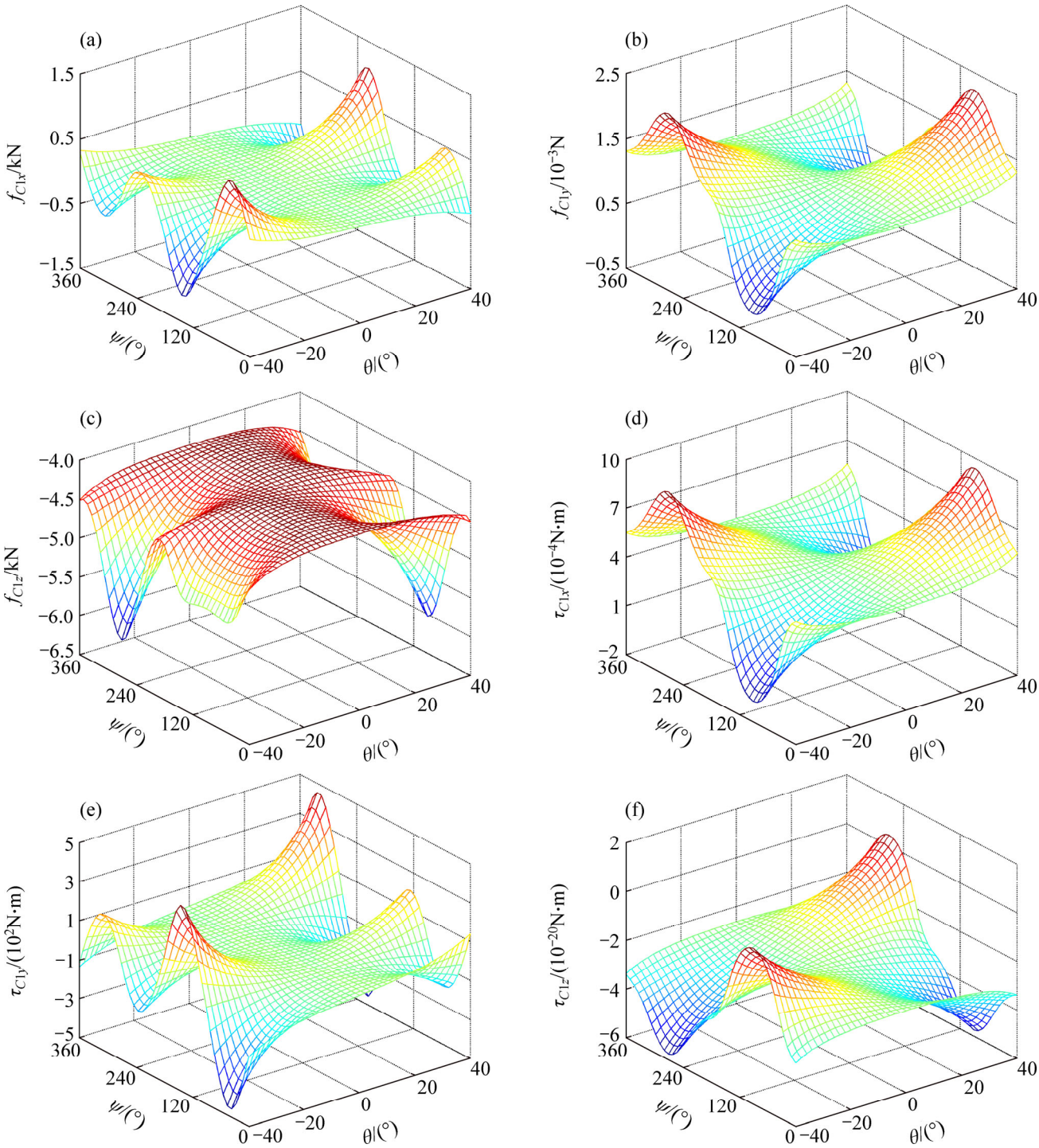

Fig. 10 Distributions of reactions in R joint over working plane at p_z=875 mm: (a) Reaction along x axis, f_{C1x}; (b) Reaction along y axis, f_{C1y}; (c) Reaction along z axis, f_{C1z}; (d) Reaction about x axis, τ_{C1y}; (e) Reaction about y axis, τ_{C1y}; (f) Reaction about z axis, τ_{C1z}

From Fig. 10, it can be seen that the reaction forces in three directions vary noticeably with the configuration parameters. Meanwhile, the reaction moments about x and z axes are zero, which means that the gravity of the platform does not cause rotational deflections at the center of revolute joint. This is coincident with the fact in that the revolute joint can freely rotate about its axis (x axis) and the projection of the gravity center on limb 1 locates at the centre line of the revolute joint.

5 Conclusions

1) An analytical elastodynamic model is established with the technique of substructure synthesis. The limb assemblage flexibility is accounted into through FE formulation by treating it as a spatial beam with non-uniform cross-sections supported by two sets of lumped virtual springs of joints.

2) Based on the proposed elastodynamic model, a quasi-static analysis is conducted to predict the joint reactions and component deflections by degenerating the differential terms of the governing equations. Compared with the traditional FE method, the present method for joint reaction prediction is much more concise and effective.

3) The elastic displacements of the moving platform and reactions in the revolute and spherical joints caused by the gravity are calculated at given work configurations. The results show that the influence of the gravity on the system deflections cannot be neglected.

4) A piece-by-piece computation algorithm is proposed to predict the joint reactions throughout the workspace. The distributions of reactions in revolute and spherical joints in an individual limb assemblage are predicted to demonstrate a strong dependency of joint reactions on system configurations.

References

[1] HENNES N, STAIMER D. Application of PKM in aerospace manufacturing-high performance machining centers ECOSPEED, ECOSPEED-F and ECOLINER [C]// Proceedings of the 4th Chemnitz Parallel Kinematics Seminar. Chemnitz: Verlag Wissenschaftliche Scripten, 2004: 557−577.

[2] NEUMANN K E. Tricept application [C]// Proceedings-3rd Chemnitz Parallel Kinematics Seminar. Zwickau: Verlag Wissenschaftliche Scripten, 2002: 547−551.

[3] CACCAVALE F, SICILIANO B. The tricept robot-dynamics and impedance control [J]. IEEE, 2003, 2: 263−268.

[4] CARRETERO J A, PODHORODESKI R P, NAHON K A, GOSSELIN C M. Kinematic analysis and optimization of a new three degree-of-freedom spatial manipulator [J]. Journal of Mechanical Design, 2000, 122: 17−24.

[5] LI Yan-min, XU Qing-song. Kinematic analysis of a 3-PRS parallel manipulator [J]. Robotics and Computer-Integrated Manufacturing, 2007, 23: 395−408.

[6] POND G T, CARRETERO J A. Kinematic analysis and workspace determination of the inclined PRS parallel manipulator [C]// Proceedings of the 15th CISM - IFToMM Symposium on Robot Design, Dynamics and Control. Saint-Hubert: Springer Verlag, 2004: 1−6.

[7] CHENG X, HUANG Y M, FAN Z M, SU J H. Workspace generation of the 3-PRS parallel robot based on the NN [C]// Proceedings of the First International Conference on Machine Learning and Cybernetics. Beijing: IEEE, 2002: 4−5.

[8] GEOFFREY P, CARRETERO G A. Formulating Jacobian matrices for dexterity analysis of parallel mechanism [J]. Mechanism and Machine Theory, 2006, 41: 1505−1519.

[9] LI Qin-chuan, CHENG Zhi, CHEN Qiao-hong, WU Chuan-yu, HU Xu-dong. Parasitic motion comparison of 3-PRS parallel mechanism with different limb arrangements [J]. Robotics and Computer-Integrated Manufacturing, 2011, 27: 389−396.

[10] NIGUS H. Semi-analytical approach for stiffness estimation of 3-DOF PKM [J]. Modern Mechanical Engineering, 2014, 4: 108−118.

[11] WANG You-yu, LIU Hai-tao, HUANG Tian, CHRTWYND D G. Stiffness modeling of the tricept robot using the overall Jacobian matrix [J]. ASME Journal of Mechanisms and Robotics, 2009, 1: 021002.

[12] LI Yong-gang, SONG Yi-min, FENG Zhi-you, ZHANG Ce. Inverse dynamics of 3-RPS parallel mechanism by Newton−Euler formulation [J]. Acta Aeronautica et Astronautica Sinica, 2007, 28: 1210−1215. (in Chinese)

[13] XI Feng-feng, ANGELICO O, SINATRA R. Tripod dynamics and its inertia effect [J]. ASME Journal of Mechanical Design, 2005, 127: 144−149.

[14] WIENS G J, SHAMBLIN, S A, OH Y H. Characterization of PKM dynamics in terms of system identification [J]. Journal of Multi-body Dynamics, 2002, 216(1): 59−72.

[15] WU Pei-dong, XIONG He-gen, KONG Jian-yi. Dynamic analysis of 6-SPS parallel mechanism [J]. International Journal of Mechanics and Materials in Design, 2012, 8(2): 121−128.

[16] JI Z M. Study of the effect of Leg Inertia in Stewart Platforms [C]// Proceedings of the IEEE Conference on Robotics and Automation. Altanta: IEEE, 1993: 121−126.

[17] LEE J D, GENG Z. A dynamic model of a flexible Steward platform [J]. Computer and Structures, 1993, 48(3): 367−374.

[18] LIU Shan-zeng, YU Yue-qing, ZHU Zhen-zai, SU Li-ying, LIU Qing-bo. Dynamic modeling and analysis of 3-RPS parallel manipulator with flexible links [J]. Journal of Central South University, 2010, 17(2): 323−331.

[19] WANG Xiao-yu, MILLS J K. Dynamic modeling of a flexible-link planar parallel platform using a substructuring approach [J]. Mechanism and Machine Theory, 2006, 41(6): 671−687.

[20] ZHANG Xu-ping, MILLS J K, CLEGHORN W L. Dynamic modeling and experimental validation of a 3-PRR parallel manipulator with flexible intermediate links [J]. Journal of Intelligent and Robotic Systems, 2007, 50(4): 323−340.

[21] SHIAU T N, TSAI Y J, TSAI M S. Nonlinear dynamic analysis of a parallel mechanism with consideration of joint effects [J]. Mechanism and Machine Theory, 2008, 43(4): 491−505.

(Edited by DENG Lü-xiang)